

Journal of Materials Chemistry C

Accepted Manuscript



This is an *Accepted Manuscript*, which has been through the Royal Society of Chemistry peer review process and has been accepted for publication.

Accepted Manuscripts are published online shortly after acceptance, before technical editing, formatting and proof reading. Using this free service, authors can make their results available to the community, in citable form, before we publish the edited article. We will replace this *Accepted Manuscript* with the edited and formatted *Advance Article* as soon as it is available.

You can find more information about *Accepted Manuscripts* in the [Information for Authors](#).

Please note that technical editing may introduce minor changes to the text and/or graphics, which may alter content. The journal's standard [Terms & Conditions](#) and the [Ethical guidelines](#) still apply. In no event shall the Royal Society of Chemistry be held responsible for any errors or omissions in this *Accepted Manuscript* or any consequences arising from the use of any information it contains.

Highly-luminescent dual mode rare-earth nanorods assisted multi-stage excitable security ink for anti-counterfeiting applications[†]Pawan Kumar^a, Jaya Dwivedi^a and Bipin Kumar Gupta^{*,a}

5 Received (in XXX, XXX) XthXXXXXXXXX 20XX, Accepted Xth XXXXXXXXXXXX 20XX

DOI: 10.1039/b000000x

Herein, we report the synthesis of multi-stage excitable (379 nm, 980 nm and 1550 nm) highly-luminescent Y₂O₃:Yb³⁺, Er³⁺ nanorods by hydrothermal method which can emit both hypersensitive green (562 nm) and strong red (660 nm) in a single host lattice for transparent security ink application. Moreover, these luminescent nanorods also exhibit both down-shifts (1127 nm) as well as upconversion (562 nm) features at a single excitation NIR wavelength of 980 nm. We explored the characterizations of these luminescent nanorods by studying their structural/microstructural, photoluminescence and time-resolved spectroscopic techniques. Furthermore, these luminescent nanorods have exhibited the tuning of emission colours from red to green by controlling the sintering temperature. We demonstrated that these novel luminescent nanorods offer new opportunities for making high-end multi-stage excitable transparent security ink. The state-of-art production process of ink is facile and it is most suitable for bulk production at an economical cost. Hence, the security inks can have remarkable global applications for protection against counterfeiting deeds.

Introduction

Recently, data security has become an important issue of contemplation for each sector of industry as well as in the government offices in the contemporary world. The increasing trend of counterfeiting has become more common in all walks of our life and it is causing significant damage and as well as posing serious security threats to individuals, companies, and nation on the whole. The counterfeiting of currency has detrimental effect on socio-economic processes of a society which leads to reduction in the value of currency. The counterfeiting in the medicine sector can severely jeopardizes human health, whereas, counterfeiting of documents is infringement of the copyright laws. Consequently, governments and private industries, all over the world have to bear a loss of billions of dollars annually due to illegal counterfeiting activities.¹⁻⁵ Currently, one of the major issues is to completely check the counterfeiting of currency as well as important documents including those related to strategic sectors of any nation. During the last decade, millions of dollars have been spent worldwide by governments and industries to safeguard their products and currencies from being counterfeited and the efforts have yielded positive results. Almost, every country has opted for protection against fake currencies by either through holographic technique or through visible luminescent ink or bands etc. (which glow under UV light).⁶⁻¹⁰ Furthermore, commercial and industrial sectors; particularly those producing branded goods and pharmaceuticals, have also adopted and have

been benefitted tremendously from these safety measures against counterfeiting.^{11, 12} Beside this, another area of security where a more overt colorimetric indicator can be used is food security, where sensing the presence of oxygen is a principal goal – the area of intelligent packaging.¹³

During past decades, a number of anti-counterfeiting technologies like simple marker, plasmonic security labels, holograms and security inks etc. were developed as a shield against counterfeiting.^{10,14} Now a day, the development of new materials for anti-counterfeiting has attained immense attention for their use in protection and detection of counterfeiting. However, from security point of view, the luminescent materials provide improved security due to their unique physical, chemical and optical properties. Although, there are many semiconductor nanoparticle such as CdS, CdSe, CdTe etc. which have been reported as luminescent security ink but they have their own disadvantage like toxicity, broad emission and solubility in harmful solvent. The formation of stable and transparent solution of these nanoparticles is also a difficult task. Moreover, the lanthanide doped phosphors have many advantages over these materials like low toxicity, sharp emission and solubility. Therefore, the lanthanide based transparent security ink has become a lucrative tool for security labels, identification markers and barcode system.

Our earlier efforts were to develop red emitting down shift invisible security ink based on (polyvinyl alcohol) PVA as well as sodium hexametaphosphate (SHMP) medium and successful demonstration of their use in terms of security coding.² Efforts are being made by several groups in same stream line to develop either upconversion or downconversion security ink based on lanthanide materials.⁴⁻⁵ Only single stage coding capability have been achieved by using these luminescent materials. This implies that the developed luminescent fluorophores can be excited by a single wavelength which subsequently emits only at a single wavelength. This coding technique appears comparatively less effective in order to protect the documents. Owing to this reason, a high performance multi-stage coding with many excitations and at least two colour emissions is much awaited for a long time. To develop a phosphor having all the above desirable properties at an economical cost is a great challenge in this area which is being addressed in the present investigations. Now in the present investigations, our purpose is to develop a transparent security ink with multi-stage coding in a single host based highly luminescent nanostructure which is not only economic but also beneficial for high end protection. Earlier, several attempts have been made but their protection techniques were common and utilized single stage protection. Even now a days, many groups are trying the dual mode emission by incorporating two or more kinds of activator in a single host, although their intention was entirely different, because incorporating many activators is an expensive technique as well as dispersion is also an important issue.¹⁵ We have developed a single host lattice based luminescent material with single activation which can emit both up-conversion as well as down-conversion simultaneously. As a result, it provides multi-stage coding in a host. Moreover, the choice of the material for security ink applications depends upon the physical and chemical properties as well as the morphology of nanomaterials. The yttrium oxide (Y_2O_3) is an attractive host for security inks application due to its physical, chemical and optical properties. Additional advantage of using nanorods is that it also helps to bring down the amount of material required for their use in security inks application, thus reducing the production cost as well as rod shape is good in-fillers in cellulose ink matrix.¹⁶ On the basis of this concept, we have developed highly luminescent nanorods based multi-stage excitable and transparent inks for security applications.

In this study, we demonstrate the development of multi-stage excitable (379 nm, 980 nm and 1550 nm) highly luminescent $Y_2O_3:Yb^{3+}, Er^{3+}$ nanorods by using hydrothermal technique for security inks, which can intensely emit hypersensitive green and strong red colour. Furthermore, these nanorods have also depicted both down-shifts as well as upconversion nature for a single excitation wavelength at 980nm which is merely reported for such applications. We have fully characterized these luminescent nanorods by studying their gross structural, morphological, microstructural, photoluminescent and time-resolved spectroscopic techniques. We have also demonstrated the promising use of these luminescent nanorods based transparent security ink for security codes on black paper

using standard screen printing technique as well as security spot mark on currency for high end protection application which exhibits a new paradigm shift in luminescent security ink applications.

60 Experimental section

The precursors; Y_2O_3 (99.99%), $Er(NO_3)_3 \cdot 5H_2O$ (99.99%), $YbCl_3 \cdot 6H_2O$ (99.99%) and N-cetyl-N,N,N trimethyl ammonium bromide ($C_{19}H_{42}BrN$, CTAB) were purchased from Sigma-Aldrich. All reagents were of analytical (AR) grade and used as received without further purification. Double distilled water was used throughout the experiments.

The $Y_2O_3:Yb^{3+}, Er^{3+}$ nanorods were synthesized using hydrothermal method. The precursors; Y_2O_3 (99.99%), $Er(NO_3)_3 \cdot 5H_2O$ (99.99%), $YbCl_3 \cdot 6H_2O$ (99.99%) and N-cetyl-N,N,N trimethyl ammonium bromide ($C_{19}H_{42}BrN$, CTAB) were purchased from Sigma-Aldrich. The nanorods were doped with optimized concentration of rare-earth ions (1mol% of Er and 2 mol% of Yb). The stoichiometric amount of Y_2O_3 was dissolved in nitric acid followed by stirring at 80°C temperature until solution turned into a transparent nitrate solution. The precursors $Er(NO_3)_3 \cdot 5H_2O$, $YbCl_3 \cdot 6H_2O$ and CTAB were dissolved in deionized water. Above prepared solutions was mixed in ethanol solution (1:5 ethanol to water ratio) under vigorous stirring at room temperature. The sodium hydroxide solution was added to the above mixture solution along with magnetic stirring till pH of the final solution becomes ~12. We tried several statistical run with different pH value and ultimately, we found that pH ~12 favours the reaction for long uniform nanorods. Further, this solution was transferred into a sealed hydrothermal bomb which is kept at 185°C for 10 hours in a box furnace. The obtained precipitate was centrifuged several times with de-ionized water at 5000 rpm and then dried at 100°C. The final product was heated at 1000°C in a box furnace for 6 hours. In this method, the yield of material was more than 90% with a high degree of homogeneity throughout the sample.

A standard PVC gold medium (locally fabricated, printing ink manufactured by Commercial Techno Colours, Ram Nagar, Varanasi-221005, India) was used to disperse the as-synthesized dual mode $Y_2O_3:Yb^{3+}, Er^{3+}$ nanorods for security printing application. The commercial PVC gold medium used in the present investigation is shown in Fig. S1(see supporting information). The choice of dispersive medium is important for two purposes, firstly to disperse rare-earths into the medium without formation of clusters or agglomerates of nanorods and secondly, for obtaining better printing, the viscosity of medium (3000 micro poise) is very important which provides sticky nature with printing paper. Our earlier efforts using PVA as medium failed to avoid formation of clusters.²In a typical experiment, a commercially purchased 50 ml PVC gold medium solution was taken in beaker and 200 mg $Y_2O_3:Yb^{3+}, Er^{3+}$ nanorods were mixed with solution. The resultant mixture was sonicated at 45 kHz frequency for 30 min to obtain proper dispersion. The highly transparent (~81%) colloidal solution was obtained which is shown in Fig. S2 (see supporting information).

To make a pattern onto black paper, we used a standard screen printing technique for object printing as well as for alphabets.

The gross crystal structure analysis of sample was carried by using X-ray powder diffraction (XRD) with Bruker AXS D8 Advance X-ray diffractometer, using Cu $K\alpha_1$ radiation ($\lambda = 1.5406 \text{ \AA}$). The ultraviolet (UV) absorption spectra were recorded by UV-visible spectrometer (Model 160 UV Shimadzu). Thermo gravimetric analysis was done by thermal analysis instrument having a heating rate of $10 \text{ }^\circ\text{C min}^{-1}$ in an air flow of 100 mL min^{-1} . Raman studies were carried out using Renishaw inVia Raman spectrometer, UK with an excitation source of 785 nm . The surface morphology and energy dispersive X-ray (EDAX) was examined by using Carl ZEISS EVOR-18 equipment at 10 kV operating voltage. Transmission electron microscopy and high-resolution transmission microscopy micrographs were recorded by using Tecnai G2 S-Twin transmission electron microscope with a field emission gun operating at 300 kV . The photoluminescence and time-resolved spectroscopy were carried out using Edinburgh spectrometer, where Xenon lamp acts as source of excitation. The PL mapping of luminescent nanorods was performed by WITech alpha 300R+ Confocal PL microscope system (WITechGnBH, Ulm, Germany), where 375 , 980 and 1550 nm diode lasers acts as a source of excitations. The NIR emissions above 1100 nm were taken by NIR detector. The fluorescent images were recorded by using Nikon ECLIPSE 80i spectrometer.

Results and discussion

A novel strategy has been adopted to synthesize highly luminescent $\text{Y}_2\text{O}_3:\text{Yb}^{3+}, \text{Er}^{3+}$ nanorods by customized hydrothermal method. The proper interaction between the dopant (Yb^{3+}) and co-dopant (Er^{3+}) is very important to obtain highly-efficient luminescent materials. Here, the optimization of concentration is playing key role to get bright photoluminescent material. The addition of Yb^{3+} ion increases the absorption because the Yb^{3+} ion efficiently absorbs the energy and get excited. The excited Yb^{3+} ion transfers this energy to Er^{3+} ion which promotes its own electrons in higher energy level as shown in Fig. S3 (see supporting information). Subsequently, the population in excited states of Er^{3+} increases significantly. The energy transfer sturdily depends upon the doping concentration of both dopant as well as co-dopant. Our main focus of the present investigation is to optimize the green PL emission intensity of $\text{Y}_2\text{O}_3:\text{Yb}^{3+}, \text{Er}^{3+}$ nanorods while keeping the concentration of Yb^{3+} fixed. The PL intensity of the green emission was varied with respect to change in concentration of Er^{3+} from 0.5 to $2.5 \text{ mol } \%$ at fixed concentration of Yb^{3+} ($2 \text{ mol } \%$) (supporting information Fig. S4). The optimum concentration of Er^{3+} was obtained at $\sim 1 \text{ mol } \%$. Further, the optimum concentration of Yb^{3+} was also investigated from 1 - $3 \text{ mol } \%$ at fixed optimum concentration of Er^{3+} $\sim 1 \text{ mol } \%$. We found that the efficient energy transfer with high green emission was obtained at $2 \text{ mol } \%$ as shown in Fig. S5 (see supporting information). Thus the optimum concentration of dopant and co-dopant were obtained: $\text{Yb}^{3+} \sim 2 \text{ mol } \%$, $\text{Er}^{3+} \sim 1 \text{ mol } \%$ for $\text{Y}_2\text{O}_3:\text{Yb}^{3+}, \text{Er}^{3+}$ nanorods.

The same optimum concentration of the sample also exhibits unique features in terms of down shift with a strong green emission at 562 nm upon 379 nm excitation wavelength. Moreover, we have also demonstrated the energy level diagram of optimum sample for down-shift in Fig. S6 (see supporting information). Further, luminescent nanorods synthesized with the optimum concentration were fully characterized through several structural/microstructural and spectroscopic techniques.

The crystalline structure of $\text{Y}_2\text{O}_3:\text{Yb}^{3+}, \text{Er}^{3+}$ nanorods were investigated by using X-ray powder diffraction ($\text{CuK}\alpha_1$; $\lambda=1.5406 \text{ \AA}$). Fig. 1a shows the XRD pattern of 1000°C heat treated $\text{Y}_2\text{O}_3:\text{Yb}^{3+}, \text{Er}^{3+}$ nanorods. The XRD result exhibits that nanorods have cubic phase with good crystallinity (as per JCPDS card no. 43-1036). The estimated lattice parameters for $\text{Y}_2\text{O}_3:\text{Yb}^{3+}, \text{Er}^{3+}$ nanorods were $a = b = c = (10.5869 \pm 0.0043) \text{ \AA}$ which are comparable to standard lattice parameters $a = b = c = 10.6040 \text{ \AA}$. The inset of Fig. 1a shows the proposed crystal structure of Y_2O_3 where Y atoms are replaced by Er and Yb atoms. Fig.1b represents the Raman spectrum of luminescent nanorods. The result of Raman spectrum reveals that the host lattice has bands at 377 cm^{-1} , 428 cm^{-1} , 465 cm^{-1} , 511 cm^{-1} and 541 cm^{-1} . The band present at 377 cm^{-1} represents the cubic phase of $\text{Y}_2\text{O}_3:\text{Yb}^{3+}, \text{Er}^{3+}$ nanorods. The obtained results are in good agreement with the earlier reports on Raman spectrum of Y_2O_3 host.¹⁷ Fig.1c demonstrates FT-IR spectrum of nanorods sintered at 1000°C as well as as-synthesized nanorods at 185°C .

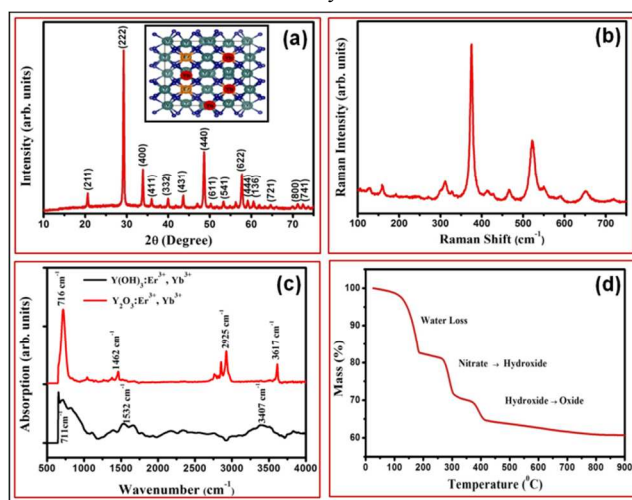


Fig. 1(a) XRD patterns of 1000°C treated $\text{Y}_2\text{O}_3:\text{Yb}^{3+}, \text{Er}^{3+}$ nanorods. The right inset shows proposed model of cubic cell of the structure of $\text{Y}_2\text{O}_3:\text{Yb}^{3+}, \text{Er}^{3+}$ nanorods, (b) shows the Raman spectrum of $\text{Y}_2\text{O}_3:\text{Yb}^{3+}, \text{Er}^{3+}$ nanorods, (c) the FT-IR spectrum of $\text{Y}_2\text{O}_3:\text{Yb}^{3+}, \text{Er}^{3+}$ nanorods and (d) thermogravimetric analysis (TGA) of $\text{Y}_2\text{O}_3:\text{Yb}^{3+}, \text{Er}^{3+}$ nanorods.

The FT-IR spectrum of heated nanorods at 1000°C shows no peak around 3400 cm^{-1} due to absence of OH group, which suggests that the hydroxide formed ($\text{Y}(\text{OH})_3:\text{Yb}^{3+}, \text{Er}^{3+}$) at 185°C during hydrothermal process is completely converted into oxide form ($\text{Y}_2\text{O}_3:\text{Yb}^{3+}, \text{Er}^{3+}$) on sintering temperature at 1000°C .

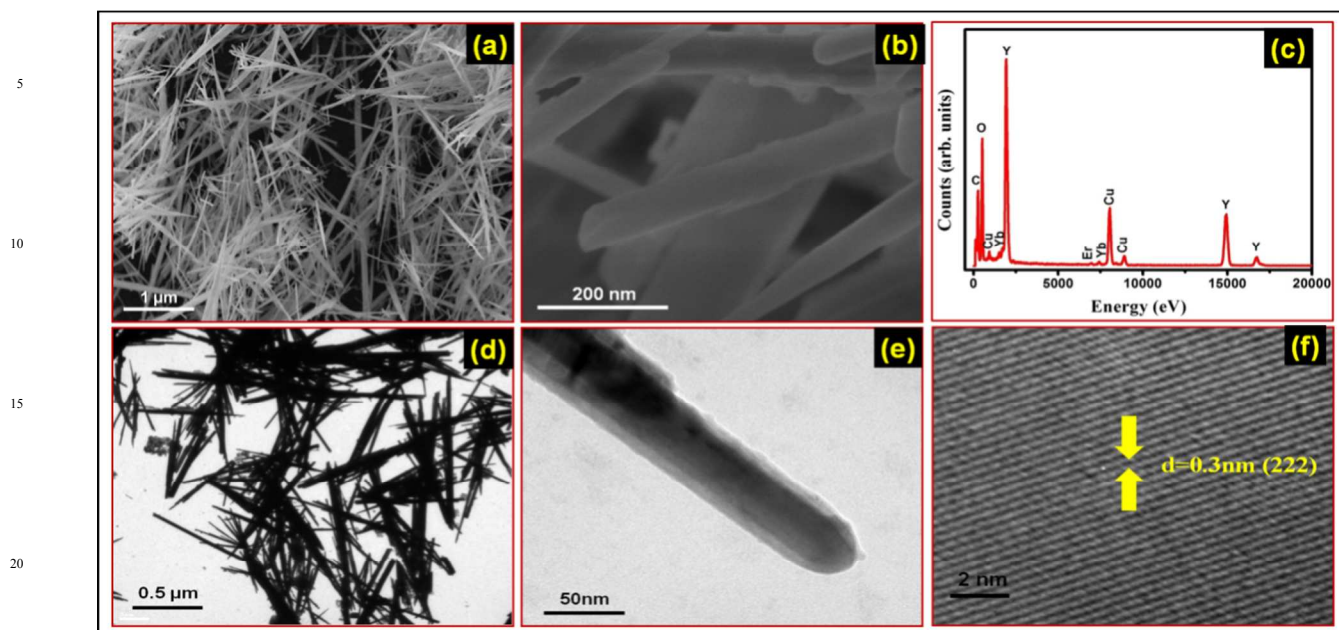


Fig. 2(a) & (b) show the SEM images of $\text{Y}_2\text{O}_3:\text{Yb}^{3+}$, Er^{3+} nanorods and magnified view of Fig. (a) respectively, (c) exhibits the EDAX analysis of $\text{Y}_2\text{O}_3:\text{Yb}^{3+}$, Er^{3+} nanorods, (d) & (e) exhibit the typical TEM image of nanorods and single nanorods respectively and (f) HRTEM of $\text{Y}_2\text{O}_3:\text{Yb}^{3+}$, Er^{3+} nanorods.

It is well known that the surface to volume ratio in case of nanorod is larger than spherical particle. The rare-earth ions near the surface have large numbers of unsaturated bond, which ultimately leads to surface defects and reaction with OH-group. Consequently, the luminous intensity of as-synthesized nanorods is lower as compared to heat-treated nanorods. This indicates that the luminescence increases due to absence of OH group in $\text{Y}_2\text{O}_3:\text{Yb}^{3+}$, Er^{3+} nanorods.¹⁸ To understand the thermal decomposition of as-synthesized $\text{Y}_2\text{O}_3:\text{Yb}^{3+}$, Er^{3+} nanorods, the thermogravimetric analysis (TGA) investigation was carried out. Fig. 1d exhibits the TGA analysis of $\text{Y}_2\text{O}_3:\text{Yb}^{3+}$, Er^{3+} nanorods, which demonstrate the three temperature interludes corresponding to three substantial weight loss processes. The first interlude between 100-182°C corresponds to water loss. The interlude between 270-310°C is due to decomposition of nitrates into hydroxides. The last interlude between 370°C and 410°C is due to the decomposition of hydroxide into oxide. The obtained result is consistent with earlier reported results.¹⁹

The surface morphology was examined by using scanning electron microscope. Fig. 2a demonstrates the SEM image of nanorods. The image shows that the synthesized nanorods have highly dense nanostructure with uniform size distribution. The magnified version of SEM image of nanorods is shown in Fig. 2b which clearly demonstrates the dimensions of nanorods which are in the range of nanometers: 50-90 nm diameter and length ~ 1-3 μm at optimum growth condition (1000°C for 6 hours). The morphology of these luminescent materials are originated in rod shape due to the initial nucleation of hexa-hydroxy phase formation during intermediate reaction (after hydrothermal

process before final sintering at 1000°C for oxide phase formation) where nitrates solution of metals converted into hydroxy phase at 185°C as shown in Fig. S7 (see supporting information). The surface morphologies of $\text{Y}_2\text{O}_3:\text{Yb}^{3+}$, Er^{3+} nanorods at different time intervals during growth temperature at 1000°C and statistic histogram of size distribution are shown in Figs. S8-S9 (for more details, see supporting information). The different growth temperature was employed to optimize the luminescence behaviour as well as controlled morphologies. The energy-dispersive X-ray analysis (EDAX) is performed for the element detection. Fig. 2c demonstrates the elemental analysis of nanorods which confirmed the presence of Y, O, Er and Yb elements. The microstructural analysis of synthesized nanorods was done by transmission electron microscopy. Fig. 2d shows the typical TEM micrograph of nanorods. The TEM micrograph of an individual nanorod is shown in Fig. 2e. A typical HRTEM micrograph of nanorods in Fig. 2f exhibits that the nanorods have well resolved lattice fringes without distortion which represents the good crystal quality. The estimated d-spacing of nanorods is ~0.302 nm which is comparable to the 0.306 nm corresponding to (222) plane (JCPDS card no. 43-1036).

The photoluminescence and time-resolved spectroscopy were carried out to explore spectroscopic features of luminescent nanorods which legitimate its potential use for high-end security ink applications. The emission spectrum of $\text{Y}_2\text{O}_3:\text{Yb}^{3+}$, Er^{3+} nanorods at 980 nm excitation is shown in Fig. 3a. The emission spectrum demonstrates that there are two emission bands; one band having a peak at 562 nm (green emission) and another at 660 nm (red emission). The green band corresponds to ${}^2\text{H}_{11/2}$, ${}^4\text{S}_{3/2} \rightarrow {}^4\text{I}_{15/2}$ transition whereas the red emission band is a

consequence of ${}^4F_{9/2} \rightarrow {}^4I_{15/2}$ transition. The emission intensity of green emission is greater than red emission. The upconversion in $Y_2O_3:Yb^{3+}, Er^{3+}$ nanorods can be explained by two mechanisms, energy transfer (ET) and excited state absorption (ESA).²⁰⁻²² The Yb^{3+} ion absorb the laser photon and transfer this energy to Er^{3+} ion; due to this the population at ${}^4I_{11/2}$ increases. The populated ${}^4I_{11/2}$ level is further excited by three processes; excited state absorption (ESA), energy transfer from neighbouring Er^{3+} ion and energy transfer from Yb^{3+} ion. The excited ${}^4F_{7/2}$ level usually relaxes non-radiatively to two lower energy levels; ${}^2H_{11/2}$ and ${}^4S_{3/2}$. The radiative emission from ${}^2H_{11/2}$ and ${}^4S_{3/2}$ energy levels to ground state ${}^4I_{15/2}$ produces the green emission. The populated ${}^4F_{7/2}$ level also relaxes non-radiatively to ${}^4I_{13/2}$. The ${}^4I_{13/2}$ level is excited to ${}^4F_{9/2}$ level by the same mechanism as described above. The ${}^4F_{9/2}$ level relaxes radiatively which causes red emission. Fig. 3b demonstrates the emission spectra at excitation at 980 nm in NIR region. The result demonstrates that the $Y_2O_3:Yb^{3+}, Er^{3+}$ nanorods have a strong emission peak at 1127 nm, corresponding to excitation at 980 nm which is merely reported in literature. Additional, interesting feature of $Y_2O_3:Yb^{3+}, Er^{3+}$ nanorods is shown in Fig. S10 (see supporting information), where emission spectrum exhibits the down shift characteristic of $Y_2O_3:Yb^{3+}, Er^{3+}$ nanorods in the NIR range of 1300-1700 nm at 980 nm excitation wavelength which is not reported earlier till date for this system. Fig. 3c shows the CIE color coordinates corresponding to emission at 980 nm with values $x=0.3880$ and $y=0.6002$. The tuning of emission wavelength from red to green is shown in Fig. 3d. Fig. 3d reveals the intensity ratio of green to red emission (I_G/I_R) at different temperature. The green colour intensity is enhanced with increase in temperature leading to an increase in the ratio.

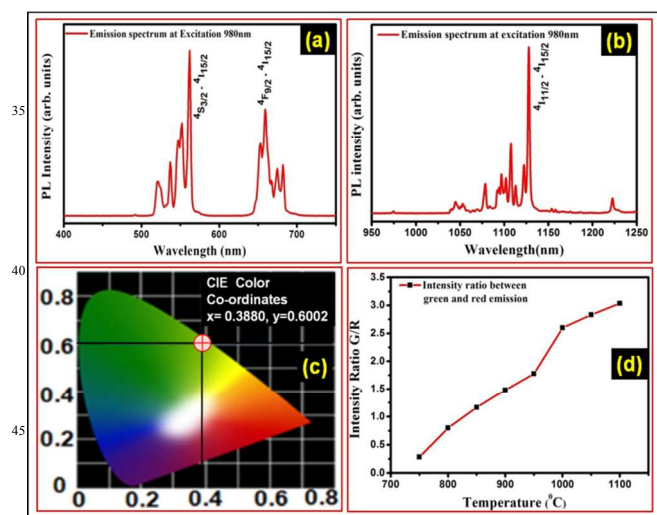


Fig. 3(a) & (b) show the photoluminescence emission spectra of $Y_2O_3:Yb^{3+}, Er^{3+}$ nanorods at excitation 980 nm, (c) demonstrates the CIE colour coordinates of green emission and (d) shows the ratio between green and red emission (I_G/I_R) with temperature.

60
65
70
75
80
85

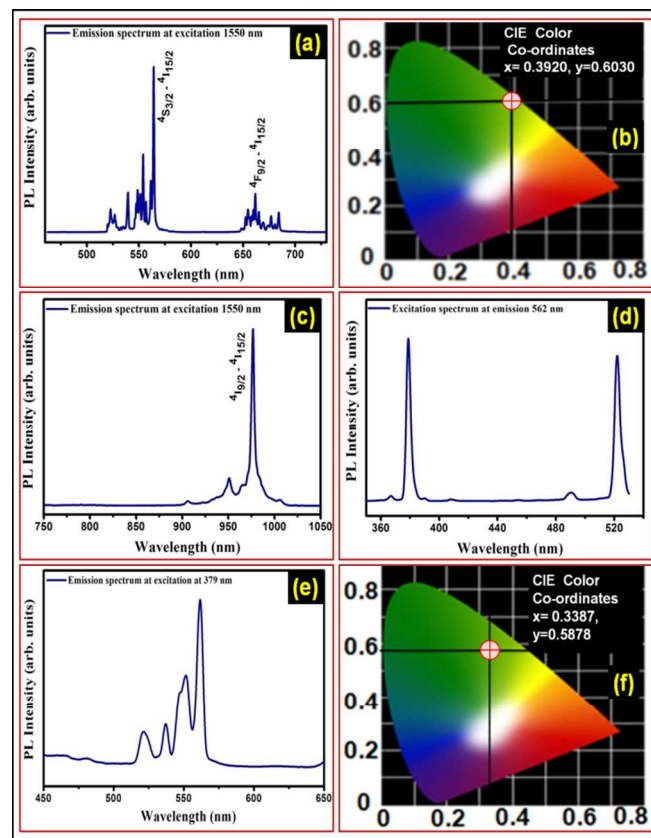


Fig. 4 (a) shows the photoluminescence emission spectrum (460-730 nm visible region) of $Y_2O_3:Yb^{3+}, Er^{3+}$ nanorods at excitation 1550 nm. (b) represents the CIE colour coordinates of green emission of $Y_2O_3:Yb^{3+}, Er^{3+}$ nanorods at excitation 1550 nm in visible region, (c) exhibits the photoluminescence emission spectrum of $Y_2O_3:Yb^{3+}, Er^{3+}$ nanorods at excitation 1550 nm in NIR region (750-1050 nm), (d) shows the excitation spectrum of $Y_2O_3:Yb^{3+}, Er^{3+}$ nanorods at emission 562 nm and (e) emission spectrum of $Y_2O_3:Yb^{3+}, Er^{3+}$ nanorods at excitation 379 nm and (f) shows CIE colour coordinates.

The Fig. 4a demonstrates the emission spectrum of nanorods having strong green emission at 564 nm corresponding to excitation wavelength at 1550 nm which is not reported till date in any literature. Fig. 4b shows corresponding CIE color coordinates with values $x=0.3920$ and $y=0.6030$. This emission provides additional high-end security in visible range which has not been used in earlier report for security ink purpose.^{4,5} Fig. 4c exhibits the emission spectrum at excitation 1550 nm in NIR region. The result demonstrates that the $Y_2O_3:Yb^{3+}, Er^{3+}$ nanorods have strong emission peak at 976 nm corresponding to excitation at 1550 nm. The upconversion behavior of $Y_2O_3:Yb^{3+}, Er^{3+}$ nanorods at 1550 nm excitation wavelength is shown in Fig. S11 (see supporting information). Fig. 4d reveals the excitation

55

Journal of Materials Chemistry C Accepted Manuscript

spectrum at emission 562 nm. The emission of $Y_2O_3:Yb^{3+}, Er^{3+}$ nanorods at excitation 379 nm is shown in Fig. 4e, where strong green emission can be easily seen which required for our security ink application purpose. Fig. 4f demonstrates the colour coordinates with values $x=0.3387$ and $y=0.5878$. Figs. S12-S13 (see supporting information) exhibit the emission spectra of $Y_2O_3:Yb^{3+}, Er^{3+}$ nanorods at excitation wavelengths of 488 and 522 nm which could be also utilized for present proposed application.

Furthermore, uniform emission from $Y_2O_3:Yb^{3+}, Er^{3+}$ luminescent nanorod was examined by fluorescent microscopic technique (Nikon ECLIPSE 80i spectrometer). Fig. 5a and b clearly exhibit high-contrast hypersensitive green and red fluorescent image of $Y_2O_3:Yb^{3+}, Er^{3+}$ nanorods at excitation wavelength of 375 nm and 980 nm (externally equipped diode lasers compatible with Nikon ECLIPSE 80i spectrometer) respectively, without auto-fluorescence from background. The obtained fluorescent result reveals that these nanorods exhibit the uniform spatial distribution of red and green colour from different points of nanorods.

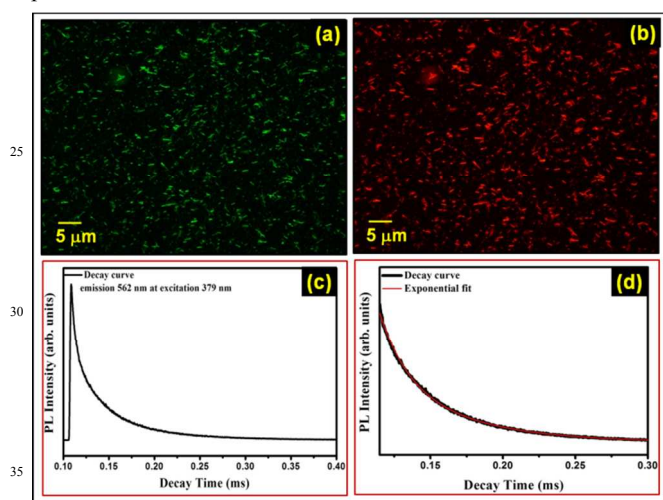


Fig. 5 (a) & (b) show the fluorescent images of $Y_2O_3:Yb^{3+}, Er^{3+}$ nanorods corresponding to excitation wavelength of 375 nm and 980 nm respectively, (c) TRPL decay profile of $Y_2O_3:Yb^{3+}, Er^{3+}$ nanorods recorded at room temperature while monitoring the emission at 562 nm at an excitation wavelength of 379 nm and (d) Exponential fitting of decay profile which gives lifetime data and the parameter generated by the exponential fitting.

The time-resolved photoluminescence (TRPL) was recorded by using a single photon counting technique with a microsecond xenon flash lamp as the source of excitation. The decay life-time is an important parameter for deciding the performance of a luminescent material and its suitable potential applications.^{24,25} The efficiency of the radiative recombination depends on the decay time of the particular transition of activator.²⁵ The luminescence decay profile as well as exponential fitting of the obtained results are shown in Figs. 5c and 5d. Fig. 5c exhibits the decay profile of $Y_2O_3:Yb^{3+}, Er^{3+}$ nanorods corresponding to excitation at 379 nm wavelength upon 562 nm emission. The life-

time data obtained from luminescent nanorods was best fitted to a double-exponential function as,

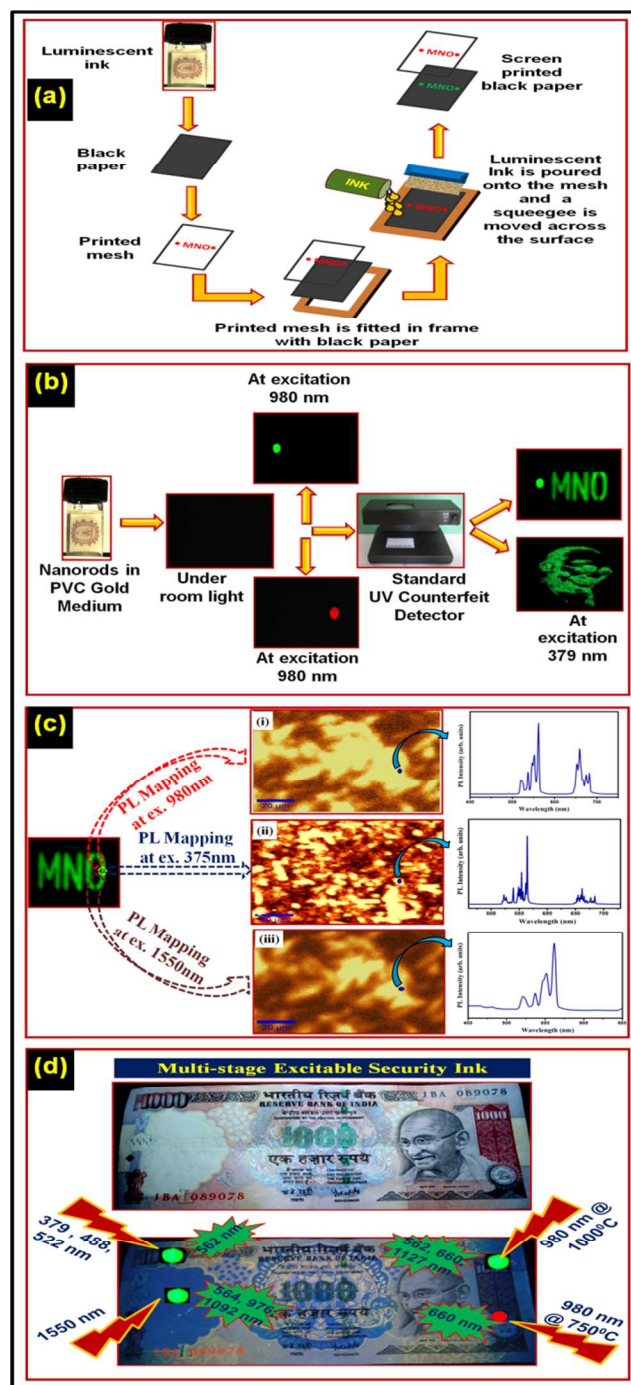


Fig. 6(a) demonstrates various steps involved in the systematic process for screen printing on black paper, (b) printed pattern images of Mahatma Gandhi and alpha bates exposed under 379 nm excitation wavelength, it can be easily seen that these images clearly show the strong green color emission and images are clearly visible, (c) the PL mapping image of the selected region

of printed alpha bates excite with multi-stage excitations wavelengths at 375, 980 and 1550 nm as shown in (i), (ii) & (iii) and their PL spectra, respectively and (d) the proposed scheme for high-end protection of Indian currencies to protect

$$I(t) = A_1 \exp(-t/\tau_1) + A_2 \exp(-t/\tau_2) \quad (1)$$

Where τ_1 and τ_2 are the decay life-times of the luminescence, and A_1 and A_2 are the weighting parameters. The Fig. 5d demonstrates the exponential fitting of decay profile as described in equation (1). The parameters generated from fitting are listed in the inset in Fig. 5d. The observed life-times are $\tau_1 \sim 18.29 \mu\text{s}$ and $\tau_2 \sim 56.47 \mu\text{s}$. For double-exponential decay, the average life-time, τ_{av} is usually tailored to substitute the various components of the luminescence life-time, which is determined by the following equation.^{23, 24}

$$\tau_{av} = (A_1 \tau_1^2 + A_2 \tau_2^2) / (A_1 \tau_1 + A_2 \tau_2) \quad (2)$$

The average life-time of $\text{Y}_2\text{O}_3:\text{Yb}^{3+}, \text{Er}^{3+}$ nanorods is calculated as $\tau_{av} \sim 52.84 \mu\text{s}$. The obtained result is highly-suitable for proposed security ink applications as well as many other optical display applications.

Finally, we demonstrated the transparent multi-stage excitable security inks application of $\text{Y}_2\text{O}_3:\text{Yb}^{3+}, \text{Er}^{3+}$ nanorods for anti-counterfeiting applications, which is not reported earlier.^{25- 27} The main advantages of using standard gold PVC medium for dispersion of luminescent nanorods are easy availability in the market at low cost, convenience of printing, highly stability and sticky nature of medium (viscosity ~ 3000 micro poise) with paper which is highly desirable for such applications. For the successful demonstration of anti-counterfeiting applications, first we synthesized the luminescent security ink. For this purpose, we incorporated specific amount of luminescent nanorods in PVC gold medium. The ratio of luminescent nanorods powder and PVC gold medium has been described in details in experimental section. In order to examine the dispersion of $\text{Y}_2\text{O}_3:\text{Yb}^{3+}, \text{Er}^{3+}$ nanorods in PVC gold medium, we excited the transparent security ink solution by 980 nm wavelength diode laser which can be tune maximum up to 0-6watt, as shown in Fig. S14 (see supporting information). We have also taken SEM image of the sample upon its dispersion into PVC gold medium as shown in Fig. S15 (see supporting information). The synthesized ink is highly-stable for several hours besides maintaining its optical transparency with higher luminescence. Further, for printing of security codes, we used standard screen printing technique. The detailed systematic process of screen printing on black paper in present investigations has been shown in Fig. 6a. We printed image of the father of nation of India, Mahatma Gandhi, alphabets and circular spot printed on black paper to demonstrate the anti-counterfeiting applications. Fig. 6b demonstrates the printed pattern under different excitation wavelengths (379 and 980 nm). The pattern is

printed on black paper using transparent security ink synthesized in present investigation which can be easily seen from Fig. 6b. The visibility of printed item is almost negligible in room light. When the printed patterns (circular spots) were excited under 980 nm laser light, it showed red and green colour emissions. Furthermore, when other printed patterns (sketch image Mahatma Gandhi, alphabets) were exposed to 379 nm excitation wavelength, it has exhibited green color emission which can be easily seen at right side of Fig. 6b. Further, we examined the fluorescent mapping of selected area of printed luminescent alphabets to validate the distribution of $\text{Y}_2\text{O}_3:\text{Yb}^{3+}, \text{Er}^{3+}$ nanorods in PVC gold medium. Fig. 6c exhibits the PL mapping of that particular area upon excitation by wavelengths 375,980 and 1550 nm as shown in Fig. 6c (i), (ii) & (iii) respectively along with their corresponding PL spectra. The clear evidence of PL and PL mapping result at various wavelengths put forward its potential use for multi-stage security ink applications to protect counterfeiting. Finally, we demonstrated a realistic scheme on the basis of obtained spectroscopic results which is a legitimate proof for its application for high-end protection of Indian currency as shown in Fig. 6d. Concisely, the obtained results reveals that $\text{Y}_2\text{O}_3:\text{Yb}^{3+}, \text{Er}^{3+}$ nanorods have good structural properties, optical properties, excellent solubility in PVC gold medium and can be easily produced at large scale for commercial printing applications. The achieved results reveal that $\text{Y}_2\text{O}_3:\text{Yb}^{3+}, \text{Er}^{3+}$ nanorods can be ultimate choice for multistage security inks application for anti-counterfeiting. Therefore, we can expect $\text{Y}_2\text{O}_3:\text{Yb}^{3+}, \text{Er}^{3+}$ nanorods to offer new perspective to fabricate low cost multi-stage security ink for advanced anti-counterfeiting applications.

Conclusions

In summary, we have successfully demonstrated the development of a novel, multi-stage excitable (379 nm, 980 nm and 1550 nm) and highly-luminescent $\text{Y}_2\text{O}_3:\text{Yb}^{3+}, \text{Er}^{3+}$ nanorods based transparent ($\sim 81\%$) security ink. These luminescent nanorods were synthesized by hydrothermal method which can be scaled-up in large quantity and it could emit both hypersensitive green and strong red in a single host lattice at different excitation wavelengths. Moreover, these nanorods have exhibited both down-shifts as well as up-conversion features upon a single excitation NIR wavelength of 980 nm. Furthermore, these luminescent nanorods have exhibited the striking features related to tuning of emission colours from red to green by controlling the sintering temperature. Thus, the integration of luminescent nanorods with suitable PVC gold medium offers new opportunities for high-end multi-stage excitable transparent security ink which is highly useful for protection against counterfeiting of important documents as well as for currencies.

Acknowledgment

The authors wish to thank Prof. R. C. Budhani, Director, N.P.L., New Delhi, for his keen interest in the work. The authors are

thankful to Prof. O.N. Srivastava (Banaras Hindu University, Varanasi) for his encouragement. Mr. Pawan Kumar gratefully acknowledged University Grant Commission (UGC), Govt. of India, for financial assistance under RGNF Research Fellowship, Award No. F1-17.1/2011-12/R GNF-SC-PUN-12604/(SA-III/Website)

Notes and references

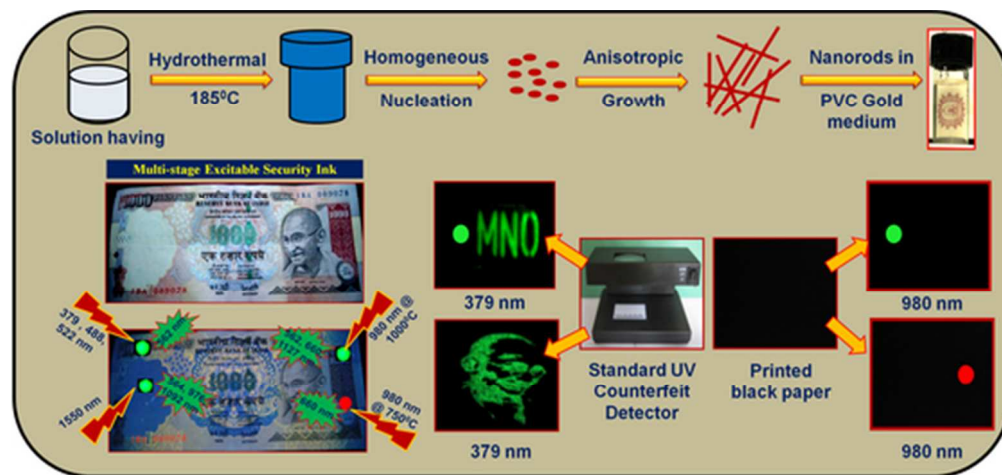
¹⁰ ^a National Physical Laboratory (CSIR), Dr. K. S. Krishnan Road, New Delhi-110012, India

* Corresponding author. Tel.: +91-11-45609385, Fx: +91-11-45609310
E-mail address: bipinbhu@yahoo.com

¹⁵ † Electronic Supplementary Information (ESI) available: [details of any supplementary information available should be included here]. See DOI: 10.1039/b000000x/

‡ Footnotes should appear here. These might include comments relevant to but not central to the matter under discussion, limited experimental and spectral data, and crystallographic data.

- (1) B. L. Volodin, B. Kippelen, K. Meerholz, B. Javidi and N. Peyghambarian, *Nature*, 1996, 83, 58-60.
- (2) B. K. Gupta, D. Haranath, S. Saini, V. N. Singh and V. Shanker, *Nanotechnol.*, 2010, 21, 055607.
- (3) S. Armstrong, O. Graydon, D. Pile and R. Won, *Nat. Photonics*, 2012, 6, 801.
- (4) W. J. Kim, M. Nyk and P. N. Prasad, *Nanotechnol.*, 2009, 20, 185301.
- (5) J. M. Meruga, W. M. Cross, P. S. May, Q. Luu, G. A. Crawford and J. J. Kellar, *Nanotechnol.*, 2012, 23, 395201.
- (6) C. E. Chesak, *Opt. Commun.* 1995, 115, 429-436.
- (7) J. Janucki and J. Owsik, *Opt. Commun.*, 2003, 228, 63-69.
- (8) A. K. Aggarwal, S. K. Kaura, D. P. Chhachhia and A. K. Sharma, *Opt. Laser Technol.*, 2006, 38, 117-121.
- (9) B. Yoon, J. Lee, I. S. Park, S. Jeon, J. Lee and J. M. Kim, *J. Mater. Chem. C*, 2013, 1, 2388-2403.
- (10) Y. Cui, R. S. Hegde, I. Y. Phang, H. K. Lee and X. Y. Ling, *Nanoscale*, 2014, 6, 282-288.
- (11) K. Huang, J. M. Carulli and Y. Makris, *Int. Conf. IEEE*, 2013.
- (12) A. K. Deisingh, *Analyst*, 2005, 130, 271-279.
- (13) A. Mills, *Chem. Soc. Rev.*, 2005, 34, 1003-1011.
- (14) R. Abargues, P. J. Rodriguez-Canto, S. Albert, I. Suarezb and P. Mart'inez-Pastor, *J. Mater. Chem. C*, 2014, 2, 908-915.
- (15) S. Chawla, M. Parvaz, V. Kumar and Z. Buch, *New J. Chem.*, 2013, 37, 3991-3997.
- (16) A. P. Singh, B. K. Gupta, M. Mishra, Govind, A. Chandra, R. B. Mathur and S. K. Dhawan, *Carbon*, 2013, 56, 86-96.
- (17) A. Ubaldini, and M. M Carnasciali, *J. Alloys Comp.*, 2008, 454, 374-378.
- (18) H. Guo and Y. M. Qiao, *Opt. Mater.*, 2009, 31, 583-589.
- (19) B. Tang, J. Ge, C. Wu, L. Zhuo, J. Niu, Z. Chen, Z. Shi and Y. Dong, *Nanotechnol.*, 2004, 15, 1273-1276.
- (20) X. Li, Q. Li, J. Wang and J. Li, *J. lumen.*, 2007, 124, 351-356.
- (21) L. Yanhoung, Z. Yongming, H. Guangyan and Y. Yongning *J. Rare Earths*, 2008, 26, 450-454.
- (22) A. Mart'neza, J. Moralesa, P. Salasb, C. Angeles-Cha'vezb, L. A. Di'az-Torresc and E. De la Rosa, *Microelectron J.*, 2008, 39, 551-555.
- (23) B. K. Gupta, N. N. Tharangattu, S. A. Vithayathil, Y. Lee, S. Koshy, A. L. M. Reddy, A. Saha, V. Shanker, V. N. Singh, B. A. Kaipparettu, A. A. Mart' and P. M. Ajayan, *Small*, 2012, 8, 3028-3034.
- (24) B. K. Gupta, T. Palanisamy, N. N. Tharangattu, L. Song, G. Wei, H. Takuya, A. L. M. Reddy, A. Saha, V. Shanker, M. Endo, A. A. Mart' and P. M. Ajayan, *NanoLett.*, 2011, 11, 5227-533.
- (25) Y. Liu, K. Ai and L. Lu, *Nanoscale*, 2011, 3, 4804-4810.
- (26) J. Wang, T. Wei, X. Li, B. Zhang, J. Wang, C. Huang and Q. *Angew. Chem. Int. Ed.*, 2014, 53, 1616-1620.
- (27) Y. Zhang, L. Zhang, R. Deng, J. Tian, Y. Zong, D. Jin and X. Liu, *J. Am. Chem. Soc.*, 2014, 136, 4893-4896.



Demonstration of new strategy for designing multi-stage excitable highly-luminescent $\text{Y}_2\text{O}_3:\text{Yb}^{3+}$, Er^{3+} nanorods based security ink for protection against counterfeiting deeds.
47x22mm (300 x 300 DPI)